Polymer 186 (2020) 122054

Contents lists available at ScienceDirect

Polymer

journal homepage: http://www.elsevier.com/locate/polymer

A new approach to phase-field model for the phase separation dynamics in polymer membrane formation by immersion precipitation method

Erlí José Padilha Júnior *, Paula Bettio Staudt, Isabel Cristina Tessaro, Nilo Sérgio Medeiros Cardozo

Departamento de Engenharia Química, Universidade Federal do Rio Grande do Sul, Porto Alegre, RS, 90040-040, Brazil

ARTICLE INFO

Keywords:
Polymer membrane
Phase separation
Phase-field model

ABSTRACT

We developed a new approach to the phase-field model to predict morphologies of polymer membranes, with the following distinctions: (i) it satisfies the Gibbs-Duhem relation and the volume fraction constraint in calculation of the driving force for diffusion; and (ii) it employs a diffusive flux equation which includes the dependence of the flux on the volume fraction of the components. The model consistency was checked by mass conservation and thermodynamic behavior. The predictions of the model were compared to Doi-Onuki (DO) and classic Cahn-Hilliard (CH) models. Differently of the DO model, the application of the proposed model was not restricted to values of initial polymer concentration inside the spinodal region. In comparison to the CH model, the main difference observed was the prediction of lower phase separation rates and minor microdomains, which may be more realistic because it considers a more appropriate approach of the driving force for diffusion and of the diffusive flux equation.

1. Introduction

In recent years, polymer membranes have been widely developed and applied for different industrial applications, such as microfiltration, ultrafiltration, reverse osmosis and gas separation [1,2]. Polymer membranes are mainly produced by phase inversion via immersion precipitation. In this process, a homogeneous polymer solution (polymer plus solvent) is cast or spun in the form of a thin film or thin-walled hollow fiber and then is immersed into a precipitation bath of non-solvent (non-solvent induced phase separation – NIPS). Due to concentration gradients, mutual diffusion of non-solvent and solvent across the interface takes place, promoting separation into a polymer-rich phase and a polymer-poor one. The polymer-rich phase becomes a solid matrix by crystallization or vitrification, containing pores originated from the polymer-poor phase [3,4]. As the membrane morphology varies significantly depending on the properties of the system components and conditions of the process, an understanding of the dynamics of the polymer membrane formation process is vital to predict and control the morphology development.

Few models are available in the literature to describe phase inversion process [5–31]. The first theoretical description of the wet-casting process was made by Cohen et al. [5], considering that chemical potential is the driving force for the process. Even though several researchers [6–13, 20,21,26] have reviewed and refined some aspects of model proposed by Cohen et al. [5], the ability of these models to provide information about the membrane microstructure is limited, because they do not directly address the phase separation process.

More recently, the researchers turned their attention to the explicit treatment of the phase separation process by a wide variety of methods, including phase-field [17–19,22,24,29–31], Lattice-Boltzmann [23], and particle simulation [14–16,25,27,28]. Among these methods, the phase-field model [32–34] is an excellent choice to simulate phase separation systems, due to some aspects that will be discussed next.

The phase-field method is based on the idea that interfaces in microstructure are diffuse and can be represented by one or more order parameters that vary smoothly (*e.g.*, concentration). This model shows the following advantages: (i) describes non-homogeneous systems without the necessity to solve high degrees of freedom that limit the size of the time step, as in methods based on particle simulation; (ii) does not require to explicitly follow the phase interfaces as in conventional multiphase methods, which requires setting boundary conditions and deriving evolution equations for each interface; (iii) implicitly incorporates physics based on curvature and manipulates the creation, destruction and fusion of interfaces, which are difficult to capture in a conventional multiphase method; (iv) does not generate anisotropy in

* Corresponding author.
E-mail address: erli@enq.ufrgs.br (E.J. Padilha Júnior).

https://doi.org/10.1016/j.polymer.2019.122054
Received 3 September 2019; Received in revised form 18 November 2019; Accepted 2 December 2019
Available online 5 December 2019

Nomenclature

d	diameter (m)
dp	percentage deviation (%)
D_i	diffusion coefficient ($m^2.s^{-1}$)
f_0	homogeneous free energy density (J)
F	total Helmholtz energy (J)
$\dot{F}$	time derivative of the Helmholtz energy of mixing ($J.s^{-1}$)
$\overline{F}$	molar quantity of Helmholtz energy ($J.mol^{-1}$)
$\underline{j}_i$	diffusive flux ($mol.m^{-2}.s^{-1}$)
l	characteristic length (m)
L	Lagrangian constraint ($m^3.s^{-1}$)
n	amount
n_t	total number of moles (mol)
np	number of parameters
P	pressure (Pa)
$\underline{r}$	refers to the position (m^3)
R	universal gas constant ($J.mol^{-1}.K^{-1}$)
R_G	radius of gyration (m)
t	time (s)
t	t test
T	temperature (K)
v	molar volume ($m^3.mol^{-1}$)
v_0	monomer molecular chain volume (m^3)
v_r	reference molar volume ($m^3.mol^{-1}$)
v_i	molar volume ($m^3.mol^{-1}$)
κ_{ij}	gradient energy coefficient ($J.m^{-1}$)
λ	multiplier (Rayleigh variational) (Pa)
μ_j	chemical potential ($J.m^{-3}$)
$\widehat{\mu}_j$	diffusion potential ($J.m^{-3}$)
M_i	mobility of pure component i ($m^5.J^{-1}.s^{-1}$)
M_{ij}	mobility of component i due to the gradient of a diffusion potential of component j ($m^5.J^{-1}.s^{-1}$)
$\underline{v}$	total (barycentric) solution velocity ($m.s^{-1}$)
$\underline{v}_i$	velocity of the component i ($m.s^{-1}$)
$\underline{v}_{med}$	medium velocity ($m.s^{-1}$)
σ^2	variance of characteristic length (m^2)
$\underline{\underline{\sigma}}^{(v)}$	viscous stress tensor ($kg.m^{-1}.s^{-2}$)
ζ	total friction coefficient density ($Pa.s.m^{-5}$)
ζ_i	friction coefficient density ($Pa.s.m^{-5}$)
ζ_0	monomer friction coefficient ($Pa.s.m^{-2}$)
υ_t	degree of freedom
Φ	potential dissipation ($J.s^{-1}$)
φ_i	volume fraction
χ_{ij}	Flory-Huggins interaction parameters
$\mathscr{R}$	Rayleigh variational ($J.s^{-1}$)
δ	functional derivative
∂	partial derivative
∇	differential
ppp	polymer-poor phase
prp	polymer-rich phase
ipc	initial polymer concentration
0	monomer
a	average
c	calculated
i	relative to component i
H	enthalpy
j	relative to component j
k	relative to component k
md	microdomain
med	medium
min	minor
n	non-solvent
p	polymer
pp	poor phase
r	reference
rp	rich phase
s	solvent
S	entropy
t	table
T	temperature
$test$	test
V	volume
φ_i	volume fraction
CA	cellulose acetate
CH	Cahn-Hilliard model
CI	confidence interval
DMF	N,N-dimethylformamide
DMSO	dimethyl sulfoxide
DO	Doi-Onuki model
FVM	finite volume method
mDO	modified Doi-Onuki model
NIPS	non-solvent induced phase separation
PES	polyethersulfone
PVDF	poly(vinylidene fluoride)
TW	this work
SDPS	surface-directed phase separation

the system, as in the lattice-Boltzmann method, which can cause a polarized morphology in some sense; (v) also captures the behavior that occurs away from the interfaces. Regarding the modeling of polymer membrane formation by NIPS, the phase-field method has the following advantages to other models: (i) a single set of equations can model the initial diffusion and the phase separation; (ii) does not imply that the polymer has to stay in the polymer solution, while the free energy barrier and low polymer mobility automatically prevent the polymer from entering the non-solvent bath; (iii) no specification of the concentrations or chemical potentials at the (polymer solution)/(non-solvent bath) interfaces is required, contrarily to what happens with most models; (iv) is easily extended to three dimensions.

There are two formulations of the phase-field model developed for modeling the polymer membranes formation by NIPS: the classic Cahn-Hilliard model [32–34] extended to multicomponent systems [18,22,24,31] and the Doi-Onuki formalism [35] expanded to multicomponents by Tree et al. [30]. In spite of their unquestionable contributions and exceptional features regarding the simulation of phase separation, these models lead to different results and have not yet provided a definitive physical elucidation of the morphological diversity of polymer membranes.

An important shortcoming of these formulations is that they assume the variational derivative of free energy to volume fraction ($\delta F/\delta\varphi_i$) as the driving force for diffusion. This is incorrect for a multicomponent system, which must obey the volume fraction constraint and the Gibbs-Duhem relationship (which affirms that when the components are restricted, their chemical potentials are also limited) [36–38]. The correct form of driving force will be discussed in Section 2.2.

In this study, motivated by the studies of Nauman and He [36,37], Cogswell and Carter [38] and Emmanuel et al. [39], which examined the phase separation involving multicomponents, we developed a new approach to the diffusion equations of phase-field model in a multicomponent system. The distinguishing features of this new approach are: (i) thermodynamical consistency, in the sense that it satisfies the

Gibbs-Duhem relation and the volume fraction constraint; (ii) the use of a diffusive flux equation in which the dependence of the flux on the volume fraction of the components is taken into consideration. The consistency of the proposed model was checked based on the mass conservation law and thermodynamical aspects. The model was also compared to models suggested by Zhou and Powell [24] and Tree et al. [30] by spinodal decomposition in the presence of an interface with a non-solvent bath. In this first moment, we focus only on the diffusive effects of phase separation.

2. Modeling

2.1. Usual approaches

2.1.1. Classic Cahn-Hilliard model

The classic Cahn-Hilliard equation [32–34] has been employed by Barton and McHugh [18], Saxena and Caneba [22], Zhou and Powell [24], and Hopp-Hirschler and Nieken [31] in the description of the phase separation process that occurs in polymer membrane formation by phase inversion.

To develop this model, initially, a diffusive flux equation must be defined. Cahn and Hilliard [32] proposed and proved that, for an isothermal system, the chemical potential gradient, $\nabla\mu_i$, must be employed as the driving force for the diffusion flux. As shown by Gibbs, in a non-ideal mixture in equilibrium is the chemical potential that becomes uniform. Therefore, the diffusive flux of a component $\underline{j}_i$, can be expressed as:

$$\underline{j}_i = -\sum_{j=1}^{n-1} \mathrm{M}_{ij} \underline{\nabla} \widehat{\mu}_j \tag{1}$$

where $\widehat{\mu}_j$ will be called as diffusion potential of component j, also named non-homogeneous chemical potential [38], and M_{ij} is the mobility of component i due to the gradient of a diffusion potential of component j, $\widehat{\mu}_j$.

The diffusion dynamics is governed by the law of mass conservation:

$$\frac{\partial \varphi_i}{\partial t} = -\underline{\nabla} \cdot \underline{j}_i \tag{2}$$

where φ_i is the volume fraction of component i. This expression can be used in conjunction with Eq. (1) to produce the extended Cahn-Hilliard equation for multicomponent systems [18,22,24,31]:

$$\frac{\partial \varphi_i}{\partial t} = \sum_{j=1}^{n-1} \underline{\nabla} \cdot \left(\mathrm{M}_{ij} \underline{\nabla} \widehat{\mu}_j\right) \tag{3}$$

In these works the diffusion potential, $\widehat{\mu}_j$, is defined as the variational derivative of the total Helmholtz energy F concerning the volume fraction of the component j [24].

$$\widehat{\mu}_j = \frac{\delta F}{\delta \varphi_j} \tag{4}$$

Considering a ternary system formed by one non-solvent (n), one solvent (s) and one polymer (p), there are only two independent variables. Choosing polymer and solvent as independent variables, Cahn-Hilliard equations can be written as follows:

$$\begin{aligned} \frac{\partial \varphi_s}{\partial t} &= \underline{\nabla} \cdot \left(\mathrm{M}_{ss} \underline{\nabla} \frac{\delta F}{\delta \varphi_s}\right) + \underline{\nabla} \cdot \left(\mathrm{M}_{sp} \underline{\nabla} \frac{\delta F}{\delta \varphi_p}\right) \\ \frac{\partial \varphi_p}{\partial t} &= \underline{\nabla} \cdot \left(\mathrm{M}_{ps} \underline{\nabla} \frac{\delta F}{\delta \varphi_s}\right) + \underline{\nabla} \cdot \left(\mathrm{M}_{pp} \underline{\nabla} \frac{\delta F}{\delta \varphi_p}\right) \end{aligned} \tag{5}$$

Despite its importance, this model may lead to some physical inconsistences related to the use of constant mobilities, as assumed in several works, and to the coupling with Eq. (4) [22,24,30,31]. Firstly, if the mobilities are assumed constant, the flux of the components does not depend on its volume fractions (Eq. (1)), which leads to the possibility of obtaining non-zero values of flux of a component in regions where it is not present [38]. Secondly, the driving force for diffusion defined by Eq. (4) is incorrect for a multicomponent system because it does not obey the Gibbs-Duhem relation and the volume fraction constraint [36–38].

2.1.2. Doi-Onuki model

Tree et al. [30] extended the Rayleigh formalism developed by Doi and Onuki [35] to multicomponent system. In the Doi-Onuki model, each component in the system must satisfy the following mass conservation equation:

$$\frac{\partial \varphi_i}{\partial t} + \underline{\nu} \cdot \underline{\nabla} \varphi_i = -\underline{\nabla} \cdot \underline{j}_i \tag{6}$$

where $\underline{\nu}$ is the total (barycentric) solution velocity:

$$\underline{\nu} = \sum_{j=1}^{n-1} \varphi_i \underline{\nu}_i \tag{7}$$

where $\underline{\nu}_i$ is the velocity of component i.

To determine $\underline{\nu}_i$, Tree et al. [30] used the Rayleigh variational principle:

$$\mathscr{R} = \dot{F} + \Phi - \lambda L \tag{8}$$

where $\mathscr{R}$ is the Rayleigh variational, $\dot{F}$ is the time derivative of the Helmholtz energy of mixing, Φ is the potential dissipation, L is a Lagrangian constraint, λ is a multiplier [30,35].

The time derivative of Helmholtz energy was expressed as:

$$\dot{F} = \int \left[\sum_{i}^{n-1} \phi_i \underline{\nu}_i \cdot \underline{\nabla} \widehat{\mu}_i\right] \mathrm{d}\underline{r} \tag{9}$$

where $\underline{r}$ refers to the position. To obtain this equation, Tree et al. [30] used Eq. (6) to replace the time derivative of the volume fraction and employed the same definition of the variational derivative of the total free energy in relation to the volume fraction (Eq. (4)) used by Zhou e Powell [24].

The potential dissipation was defined as:

$$\Phi = \frac{1}{2} \int \left[\sum_{i}^{n} \zeta_i (\underline{\nu}_i - \underline{\nu}_{med})^2 + \underline{\sigma}^{(v)} : \underline{\nabla} \underline{\nu}\right] \mathrm{d}\underline{r} \tag{10}$$

where $\underline{\sigma}^{(v)}$ is the viscous stress tensor, $\underline{\nu}_{med}$ is the "medium velocity", and ζ_i is the friction per volume of component i. The "medium velocity" was expressed as:

$$\underline{\nu}_{med} = \frac{1}{\zeta} \sum_{i}^{n} \zeta_i \underline{\nu}_i \tag{11}$$

where $\zeta = \sum_i \zeta_i$ is the total friction density. The friction coefficient density was calculated as:

$$\zeta_i = v_0^{-1} \zeta_0 \varphi_i \tag{12}$$

where v_0 is the monomer molecular chain volume and ζ_0 is the monomer friction coefficient.

The restriction applied to the Rayleigh variational principle was the incompressibility, with the pressure P, as multiplier:

$$\lambda L = \int P(\underline{\nabla} \cdot \underline{\nu}) \mathrm{d}\underline{r} \tag{13}$$

Substituting Eqs. (9), (10) and (13) into Eq. (6), the Rayleigh variational becomes:

$$\mathscr{R} = \int \left[\sum_i^n \frac{\zeta_i}{2} (\underline{v}_i - \underline{v}_m)^2 + \frac{1}{2} \underline{\underline{\sigma}}^{(v)} : \nabla \underline{v} - P(\underline{\nabla} \cdot \underline{v}) + \sum_i^{n-1} \phi_i \underline{v}_i \cdot \underline{\nabla} \widehat{\mu}_i \right] \mathrm{d}\underline{r} \quad (14)$$

As demonstrated by Tree et al. [30], stationary values of the Rayleighian with respect to $\underline{v}_i$ produce equations of motion for the component velocities. Successive re-arrangements of the component velocity equations return a coupled set of momentum and diffusion equations. Thus, disregarding the advective effects, the following expression for the diffusion equation was obtained by Tree et al. [30]:

$$\frac{\partial \varphi_i}{\partial t} = v_0 \zeta_0^{-1} \underline{\nabla} \cdot \left[\varphi_i (1 - \varphi_i) \underline{\nabla} \widehat{\mu}_i - \varphi_i \varphi_j \underline{\nabla} \widehat{\mu}_j \right] \quad (15)$$

Considering the Stokes-Einstein relation:

$$\mathrm{M}_p = v_0 \zeta_0^{-1} \quad (16)$$

and the definition of Eq. (4), the diffusion equations presented by Tree et al. [30], in terms of polymer and solvent, can be written as follows:

$$\begin{aligned} \frac{\partial \varphi_s}{\partial t} &= \underline{\nabla} \cdot \left[\mathrm{M}_p \varphi_s (1 - \varphi_s) \underline{\nabla} \frac{\delta F}{\delta \varphi_s} - \mathrm{M}_p \varphi_s \varphi_p \underline{\nabla} \frac{\delta F}{\delta \varphi_p} \right] \\ \frac{\partial \varphi_p}{\partial t} &= \underline{\nabla} \cdot \left[\mathrm{M}_p \varphi_p (1 - \varphi_p) \underline{\nabla} \frac{\delta F}{\delta \varphi_p} - \mathrm{M}_p \varphi_p \varphi_s \underline{\nabla} \frac{\delta F}{\delta \varphi_s} \right] \end{aligned} \quad (17)$$

In these equations, as in the classic Cahn-Hilliard model, the driving force for diffusion is defined incorrectly by Eq. (4), because it does not obey the Gibbs-Duhem relation and the volume fraction constraint [36–38]. Furthermore, the consideration of just one mobility for the whole system may cause errors, since components mobilities can differ significantly. As observed by Zhou [40], a low ratio between the solvent and polymer mobilities may cause the formation of layered structure, which is not verified in polymer membranes.

2.2. Proposed approach

This chapter presents the development of new diffusion equations for the phase-field model in a multicomponent system. These equations are based on the model of Cahn and Hilliard, but satisfy the Gibbs-Duhem relation and the volume fraction constraint and include a new approach for the diffusive flux equation.

Evaluating the ternary system under study, the fundamental thermodynamic relation for the Helmholtz energy (F) at constant temperature and pressure can be written as:

$$\overline{F} = \frac{F}{n_t} = -Pv + \widehat{\mu}_n \varphi_n + \widehat{\mu}_s \varphi_s + \widehat{\mu}_p \varphi_p \quad (18)$$

where $\overline{F}$ is molar Helmholtz energy, v is molar volume, and n_t is the total number of moles in the system ($n_t = n_n + n_s + n_p$). It is convenient to set $n_t = 1$ in order that $\overline{F} = F$. It may be exposed by standard thermodynamic arguments that $\widehat{\mu}_i$ obeys a Gibbs-Duhem relation at constant temperature:

$$\sum_i \varphi_i d\widehat{\mu}_i = v \mathrm{d}P \quad (19)$$

Application of the volume fraction constraint:

$$\sum_{i=1}^n \varphi_i = 1 \quad (20)$$

in Eq. (18) to exclude φ_n, we expose that variational derivatives of F with respect to φ_i are associated to differences in diffusion potentials:

$$\left(\frac{\delta F}{\delta \varphi_s} \right)_{T,V,\varphi_p} = \widehat{\mu}_s - \widehat{\mu}_n \quad (21a)$$

$$\left(\frac{\delta F}{\delta \varphi_p} \right)_{T,V,\varphi_s} = \widehat{\mu}_p - \widehat{\mu}_n \quad (21b)$$

If local thermodynamic equilibrium is assumed, the gradients of individual diffusion potentials $\underline{\nabla} \widehat{\mu}_i$, can be related to the Gibbs-Duhem equation. The supposition of local equilibrium requires that global intensive parameters fluctuate so slowly that small neighborhoods about a point can be considered in equilibrium. For a system not at global equilibrium, the hypothesis of local equilibrium is indispensable for diffusion potential to be defined. Moreover, vdP for solids and liquids is usually very small and can be neglected for simplicity [38]. Then, the Gibbs-Duhem relation for an inhomogeneous ternary system becomes:

$$\varphi_n \underline{\nabla} \widehat{\mu}_n + \varphi_s \underline{\nabla} \widehat{\mu}_s + \varphi_p \underline{\nabla} \widehat{\mu}_p = 0 \quad (22)$$

The volume fraction constraint is applied to exclude φ_n, and Eq. (22) is rearranged to put $\nabla \widehat{\mu}_s$ on the left-hand side:

$$\begin{aligned} \underline{\nabla} \widehat{\mu}_s &= (\underline{\nabla} \widehat{\mu}_s - \underline{\nabla} \widehat{\mu}_n) - \varphi_s (\underline{\nabla} \widehat{\mu}_s - \underline{\nabla} \widehat{\mu}_n) - \varphi_p (\underline{\nabla} \widehat{\mu}_p - \underline{\nabla} \widehat{\mu}_n) \\ \underline{\nabla} \widehat{\mu}_s &= (1 - \varphi_s) \underline{\nabla} (\widehat{\mu}_s - \widehat{\mu}_n) - \varphi_p \underline{\nabla} (\widehat{\mu}_p - \widehat{\mu}_n) \end{aligned} \quad (23)$$

The diffusion potential differences can be replaced by the variational derivatives (Eqs. (21a) and (21b)), resulting in:

$$\underline{\nabla} \widehat{\mu}_s = (1 - \varphi_s) \underline{\nabla} \frac{\delta F}{\delta \varphi_s} - \varphi_p \underline{\nabla} \frac{\delta F}{\delta \varphi_p} \quad (24)$$

Similarly:

$$\underline{\nabla} \widehat{\mu}_p = (1 - \varphi_p) \underline{\nabla} \frac{\delta F}{\delta \varphi_p} - \varphi_s \underline{\nabla} \frac{\delta F}{\delta \varphi_s} \quad (25)$$

As the dynamics of component diffusion are governed by the law of mass conservation:

$$\frac{\partial \varphi_i}{\partial t} = -\underline{\nabla} j_i \quad (26)$$

An expression for the flux, j_i, is required to complete the model. The diffusive flux described in Eq. (1) is strictly limited to an ideal mixture that somehow became non-homogeneous. Thus for a non-ideal multiphase system, the diffusion flux should be written as [37,39,41]:

$$\underline{j}_i = -\sum_{j=1}^{n-1} \mathrm{M}_{ij} \varphi_i \underline{\nabla} \widehat{\mu}_j \quad (27)$$

It is understandable that the flux must be proportional to φ_i, because when the volume fraction of a component approaches zero, the flux of this component should also approach zero. If it did not depend on φ_i, it would be possible to have flux of a component without it being present, violating the mass conservation [38]. This expression for the flux can be used in conjunction with Eqs. (24)–(26) to produce the modified

$$\begin{aligned} \frac{\partial \varphi_s}{\partial t} &= \underline{\nabla} \cdot \left[\mathrm{M}_{ss} \varphi_s (1 - \varphi_s) \underline{\nabla} \frac{\delta F}{\delta \varphi_s} - \mathrm{M}_{ss} \varphi_s \varphi_p \underline{\nabla} \frac{\delta F}{\delta \varphi_p} \right] + \underline{\nabla} \cdot \left[\mathrm{M}_{sp} \varphi_s (1 - \varphi_p) \underline{\nabla} \frac{\delta F}{\delta \varphi_p} - \mathrm{M}_{sp} \varphi_s \varphi_s \underline{\nabla} \frac{\delta F}{\delta \varphi_s} \right] \\ \frac{\partial \varphi_p}{\partial t} &= \underline{\nabla} \cdot \left[\mathrm{M}_{ps} \varphi_p (1 - \varphi_s) \underline{\nabla} \frac{\delta F}{\delta \varphi_s} - \mathrm{M}_{ps} \varphi_p \varphi_p \underline{\nabla} \frac{\delta F}{\delta \varphi_p} \right] + \underline{\nabla} \cdot \left[\mathrm{M}_{pp} \varphi_p (1 - \varphi_p) \underline{\nabla} \frac{\delta F}{\delta \varphi_p} - \mathrm{M}_{pp} \varphi_p \varphi_s \underline{\nabla} \frac{\delta F}{\delta \varphi_s} \right] \end{aligned} \quad (28)$$

Cahn-Hilliard equations for a ternary system:

2.3. Complementary aspects

2.3.1. Free energy for a multicomponent system

Cahn and Hilliard [32] derived an expression for the free energy, performing a Taylor expansion in terms of the derivatives of composition. They supposed that for an inhomogeneous system the free energy depends on the composition and its derivatives. Thus, considering an isotropic symmetry and truncating the Taylor expansion up to the second order terms, the free energy functional (F) for a multicomponent system can be expressed as follows:

$$F = \int_V \left[f_0(\{\varphi\}) + \sum_{i,j=1}^{n-1} \frac{1}{2}\kappa_{ij} \underline{\nabla}\varphi_i \cdot \underline{\nabla}\varphi_j \right] \mathrm{d}V \tag{29}$$

where f_0 is the homogeneous free energy density, κ_{ij} is the gradient energy coefficient which penalizes the formation of sharp interfaces, and $\{\varphi\}$ denotes sets of $n-1$ independent volume fractions. Then the Euler-Lagrange equation can be used to find the variational derivative ($\delta F/\delta\varphi_i$) present in the diffusion equations (Eqs. (5), (17) and (28)):

$$\frac{\delta F}{\delta \varphi_i} = \frac{\partial f_0}{\partial \varphi_i} - \sum_{j=1}^{n-1} \kappa_{ij} \underline{\nabla}^2 \varphi_j \tag{30}$$

Homogeneous free energy

The homogeneous free energy density can be calculated considering the Flory-Huggins model [42–45]:

$$f_0 = RT\left(\sum_{i=1}^{n} \frac{\varphi_i}{v_i} \ln\varphi_i + \sum_{j>i} \sum_{i=1}^{n-1} \chi_{ij} \frac{\varphi_i \varphi_j}{v_r} \right) \tag{31}$$

where R is the universal gas constant, T is the temperature, χ_{ij} are the Flory-Huggins interaction parameters among the i and j components, $v_{i\ (i=n,\ s\ e\ p)}$ is the molar volume of component i, and v_r is the reference molar volume (is normally considered the lowest molar volume between the system components).

The interaction parameters, χ_{ij}, correspond to non-ideal interactions between the different components and are favorable to segregation. Although these parameters are concentration and temperature dependent, in most cases, the thermodynamic properties can be reasonably described with the constant Flory-Huggins interaction parameters [46]. These parameters can be positive or negative, reflecting the endothermic or exothermic nature of the mixing process, respectively [45].

2.3.2. Parameters

Mobility (M_{ij})

The mobility parameter is related to the movement of system components, wherein M_{ij} is the mobility of component i due to a gradient of the diffusion potential of component j, $\hat{\mu}_j$. The mobility of a pure component i is usually conceptualized by the Nernst-Einstein relation [24,47]:

$$M_i = \frac{D_i v_r}{RT} \tag{32}$$

The mutual mobility models can be classified into three types: slow model [48], fast model [49], and models based on the free volume theory of Vrentas and Duda [50–57].

The slow model is used in this study because it better reflects the slow diffusion process in viscous polymer solutions. In this model, mutual mobility (M_{ij}) is limited by self-diffusion (M_i) of the slower components of the system. According to this theory, M_{ij} are calculated as:

$$M_{ii} = \frac{M_i(M_j + M_k)}{M_i + M_j + M_k} \tag{33a}$$

$$M_{ij} = M_{ji} = \frac{-M_i M_j}{M_i + M_j + M_k} \tag{33b}$$

Gradient energy coefficient (κ_{ij})

The gradient energy coefficient (κ_{ij}) determines the influence of the composition gradient on the total free energy of the domain and is related to the formation of an interface between system components. The gradient energy coefficient is divided between enthalpic (κ_{ij_H}) and entropic (κ_{ij_S}) contributions [48,58,59]. In this study, only the enthalpic contribution is used, since it best expresses systems with polymer solutions [37]. For a ternary polymer solution system, the enthalpic contribution is calculated as [18,58,59]:

$$\kappa_{ii} = \frac{RT\chi_{ik}{R_{G_i}}^2}{3v_r} \tag{34a}$$

$$\kappa_{ij} = \kappa_{ji} = \frac{RT\left[\chi_{ik}{R_{G_i}}^2 + \chi_{jk}{R_{G_j}}^2 - \chi_{ij}\left({R_{G_i}}^2 + {R_{G_j}}^2\right)\right]}{6v_r} \tag{34b}$$

where R_{G_i} is radius of gyration of component i.

3. Methodology

The phase separation in multicomponent system was evaluated by three models: CH (classic Cahn-Hilliard model) [24], DO (Doi-Onuki model) [30] and TW (this work), represented by Eqs. (5), (17) and (28), respectively.

The analysis was performed for three systems: water/DMF/PVDF, water/acetone/CA and water/DMSO/PES. Water is the non-solvent, DMF (N,N-dimethylformamide), acetone and DMSO (dimethyl sulfoxide) are the solvents, and PVDF (poly(vinylidene fluoride)), CA (cellulose acetate) and PES (polyethersulfone) are the polymers.

The numerical solution of the phase-field models was carried out by the finite volume method (FVM), using OpenFOAM (*Open Field Operation and Manipulation*) (OpenCFD Ltd.) [60]. OpenFOAM is an open source CFD package, written in C ++. The simulation domains of tests were created using the *blockMesh* utility of OpenFOAM.

Unfortunately, the complexity of the polymer membrane formation process and computational limitations make impossible to properly describe the final morphology. Therefore, to check the proposed model consistency, two tests were performed:

(i) consistency with the law of mass conservation (i.e., no spontaneous creation or destruction of one fraction over another must take place);
(ii) consistency regarding the equilibrium behavior: simulations with an initial condition involving a homogeneous domain with concentration inside the spinodal region were performed to verify if the equilibrium concentrations are in accordance with those determined by the well-known Flory-Huggins model.

These tests were made in a homogeneous domain of 1.5 μm × 1.5 μm with initial concentrations inside the spinodal region and periodic boundary conditions; the domain was divided into square cells with sides of 0.02 μm.

The models were compared for the average polymer volume fraction in the polymer-rich phases and the morphology of the microstructures generated in two-dimensional geometry. To measure these metrics, the rich phases (*prp*) were considered those with polymer volume fraction greater than at the initial polymer concentration (*ipc*), i.e., ${\varphi_p}^{prp} > {\varphi_p}^{ipc}$.

To evaluate the morphological aspect of the isolated microstructures, software ImageJ was employed. The characteristic length (l) was used to

measure the morphological aspect. This metric was determined directly in the software ImageJ [61], using the result of *minFeret*. The average characteristic length (l_a) was related to the minor diameter of each isolated microdomain ($d_{min\,i}$) with the amount of microdomains in the simulation domain (n_{md}):

$$l_a = \frac{\sum_{i=1}^{n} d_{min\,i}}{n_{md}} \tag{35}$$

In case of a dispersed structure, the characteristic length corresponds to the diameter of the dispersed microdomain, while for a co-continuous structure it represents the length of each microdomain [62].

The domain considered to solve the problem was a rectangle of 3 μm × 6 μm. The film (polymer solution) represents 30% of the domain, occupying the lower part (1.8 μm of height). The film region is divided into square cells with sides of 0.02 μm. The non-solvent bath region is divided into 3750 cells with an aspect ratio value of 22 (Fig. 1). The initial volume fractions in the film region are listed in Table 1. The bath consisted of 0.98 of non-solvent, and 0.01 of polymer and solvent. The boundary conditions were set as periodic on the sides and as symmetrical ($\partial\varphi_i/\partial y = 0$) in top and bottom.

The parameter values used in the simulations are indicated in Table 2. The interaction parameters, diffusivity and radius of gyration values were taken from the literature [24,30,47,63], as detailed in Table 2. To enable the comparison between models, despite the Doi-Onuki model considers just mobility of polymer, we employed the mobility of solvent (M_{ss}) in diffusion equation for solvent volume fraction, and we consider M_p equal to M_{pp}.

In all simulations, a random perturbation in initial conditions is necessary to initialize the phase separation. We chose a Gaussian normal distribution about the average initial volume fraction (φ_p and φ_s) with a standard deviation of 0.005.

4. Results and discussion

4.1. Consistency check of the proposed model

Figs. 2(a) to 2(c) show the ternary phase diagrams generated by well-known Flory-Huggins model [43] for the three systems analyzed. In these ternary diagrams were plotted the initial concentration together with the final concentrations of equilibrium phases calculated from Eq. (28). It can be verified that the final equilibrium concentrations provide excellent agreement with the concentrations of binodal curve determined by the Flory-Huggins model. The equilibrium configuration of this ternary systems involves only two domains (a polymer-rich and a polymer-poor phase) connected by a single interface. Initially, spinodal decomposition does not cause an equilibrium pattern. Instead, it gives nonequilibrium structures that remain to evolve with time. This develop process is interrupted when the domain concentrations reach the binodal line and the interfaces have become constant on an absolute distance scale. Fig. 2(d) illustrates the polymer volume fraction evolution in the polymer-rich and polymer-poor phase. The polymer volume fractions in these phases tend asymptotically to equilibrium concentrations (binodal values calculated by Flory-Huggins theory).

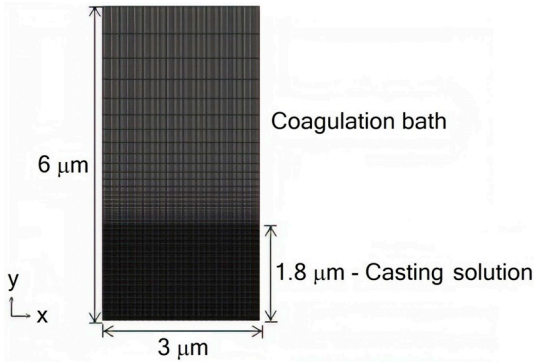

Fig. 1. Domain considered for solving the problem.

Table 1
Initial volume fractions in the film region used.

System analyzed	Nomenclature	Initial volume fraction		
		φ_n	φ_s	φ_p
water/DMF/PVDF	A1	0.6	0.2	0.2
	A2	0.05	0.75	0.2
	A3	0.05	0.55	0.4
water/acetone/CA	B1	0.1	0.7	0.2
	B2	0.05	0.55	0.4
	B3	0.2	0.4	0.4
water/DMSO/PES	C1	0.05	0.85	0.1
	C2	0.05	0.775	0.175
	C3	0.05	0.7	0.25

Table 2
Parameter values employed[a].

Parameter	Value			Unity
	water/DMF/PVDF	water/acetone/CA	water/DMSO/PES	
M_{ss}[c]	3.61×10^{-19}	3.61×10^{-19}	3.61×10^{-19}	$m^5.J^{-1}.s^{-1}$
M_{sp}[c]	-3.61×10^{-22}	-3.61×10^{-22}	-3.61×10^{-22}	$m^5.J^{-1}.s^{-1}$
M_{ps}[c]	-3.61×10^{-22}	-3.61×10^{-22}	-3.61×10^{-22}	$m^5.J^{-1}.s^{-1}$
M_{pp}[c]	7.22×10^{-22}	7.22×10^{-22}	7.22×10^{-22}	$m^5.J^{-1}.s^{-1}$
κ_{ss}	1.25×10^{-07}[b]	1.85×10^{-12}[d]	4.99×10^{-12}[d]	$J.m^{-1}$
κ_{sp}[d]	5.51×10^{-08}	1.04×10^{-08}	2.68×10^{-08}	$J.m^{-1}$
κ_{ps}[d]	5.51×10^{-08}	1.04×10^{-08}	2.68×10^{-08}	$J.m^{-1}$
κ_{pp}	1.25×10^{-07}[b]	4.16×10^{-08}[d]	1.12×10^{-07}[d]	$J.m^{-1}$
χ_{ns}	-0.06[e]	0.2[g]	-0.44[h]	–
χ_{sp}	-0.85[e]	0.5[g]	-1.41[h]	–
χ_{np}	3.5[b]	1[g]	2.7[i]	–
v_n[b]	18×10^{-6}	18×10^{-6}	18×10^{-6}	$m^3.mol^{-1}$
v_s	18×10^{-6}[b]	73.43×10^{-6}	71×10^{-6}	$m^3.mol^{-1}$
v_p	90×10^{-6}[b,f]	900×10^{-6}[f]	181×10^{-6}[f]	$m^3.mol^{-1}$

[a] $T = 300$ K.
[b] Zhou and Powell [24].
[c] The following diffusivity values were used: $D_{ss} = 10^{-10}$ $m^2.s^{-1}$ and $D_{pp} = 10^{-13}$ $m^2.s^{-1}$ [24].
[d] The following radius of gyration values were considered: $R_{g_s} = 0.2$ nm and $R_{g_p} = 30$ nm. Order of magnitude found in the literature [30,47,63].
[e] Estimated value of equation used by Zhou and Powell [24].
[f] The degree of polymerization is chosen to be small (in relation to experimental values) in the simulations in order to optimize the trade-off between the computer efficiency and model accuracy. More details in Zhou and Powell [24] and Tree et al. [30].
[g] Altena and Smolders [42].
[h] Estimated value of equation used by Barton and McHugh [18].
[i] Barton and McHugh [18].

Fig. 3 represents the component volume fractions as a function of time calculated by the proposed model (TW). It can be confirmed that the implementation of the developed model is correct, because the component volume fractions are conserved during the time.

4.2. Comparative analysis between models

The models were compared in terms of the evolution of the morphology in the simulation with the presence of an interface between the non-solvent bath and polymer solution.

The Doi-Onuki model considers just one mobility for the system. This

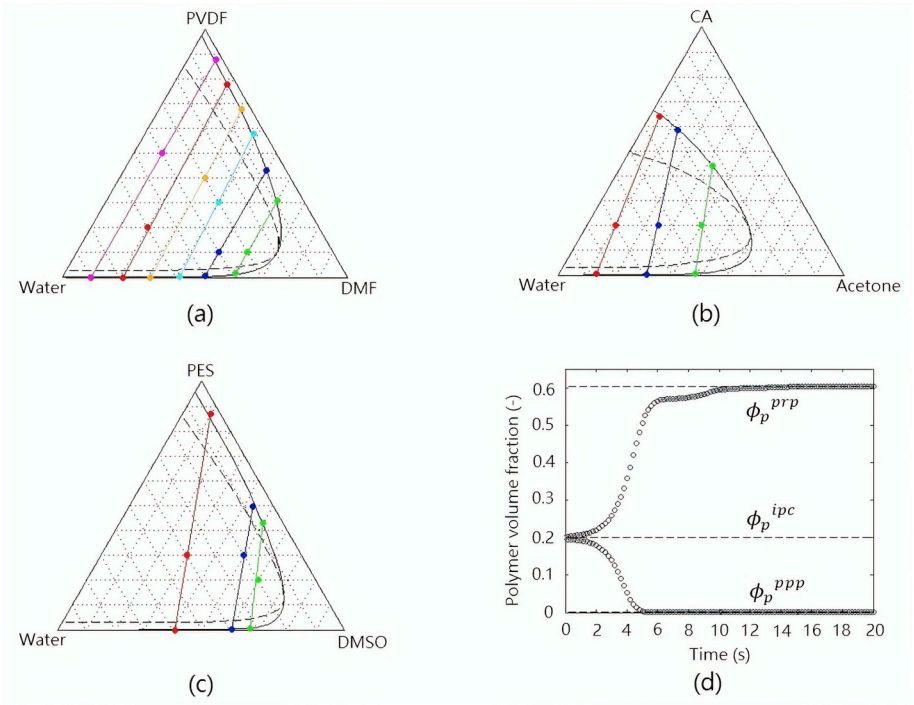

Fig. 2. Ternary diagrams with the final concentrations of equilibrium phases calculated by our model. Each diagram represent a system with different initial concentrations: (a) water/DMF/PVDF - $\{\varphi_s,\ \varphi_p\}$ = {0.1, 0.5} (pink), {0.2, 0.2} (red), {0.3, 0.4} (yellow), {0.4, 0.3} (blue), {0.5, 0.1} (darkblue), {0.6, 0.1} (green); (b) water/acetone/CA - $\{\varphi_s,\ \varphi_p\}$ = {0.1, 0.2} (red), {0.25, 0.2} (blue), {0.4, 0.2} (green); (c) water/DMSO/PES - $\{\varphi_s,\ \varphi_p\}$ = {0.3, 0.3} (red), {0.5, 0.3} (blue), {0.6, 0.2} (green). The solid line indicates the binodal and the dashed line indicates the spinodal calculated by Flory-Huggins model. Panel (d) gives polymer volume fraction in the polymer-rich and polymer-poor phase versus time for water/acetone/CA system - $\{\varphi_s,\ \varphi_p\}$ = {0.25, 0.2}. The dashed line indicates the polymer volume fractions in the binodal calculated by Flory-Huggins model. (For interpretation of the references to colour in this figure legend, the reader is referred to the Web version of this article.)

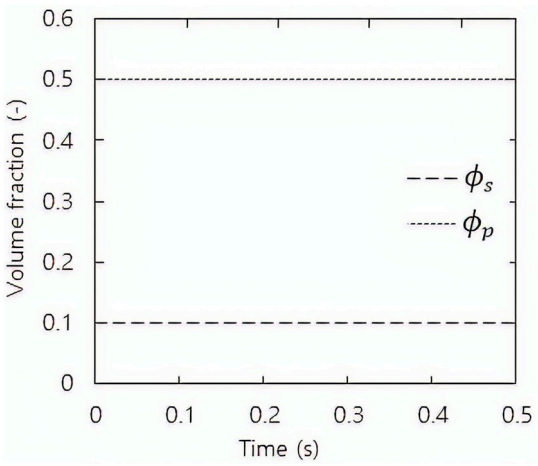

Fig. 3. Volume fraction in the simulation domain as a function of time calculated by the proposed model for water/DMF/PVDF system - $\{\varphi_s,\ \varphi_p\}$ = {0.1, 0.5}.

fact allows the formation of layered structures. Fig. 4 shows the predictions of the DO model for the morphology of water/acetone/CA system with different initial concentrations and mobilities. DO model provides adequate phase separation results only when initial concentrations of the polymer solution are inside the spinodal region (Fig. 4(a) and (b)). When the initial volume fractions are in the stable region (Fig. 4(c) and (d)) layered structures are predicted, which is not verified in the polymer membranes. For this reason, we suggest a modification in this model to adapt it to the process of membrane formation: to employ the mobility of solvent in diffusion equation for solvent volume fraction. With this change, the modified DO model (mDO) provided predictions comparable to those of the other two models.

Figs. 5–13 show comparisons between predictions of the three models for the evolution of the morphology in the film region. The simulations exhibit a morphology with two distinct phases: a polymer-rich (high φ_p) and a polymer-poor (low φ_p). CH model predicts higher phase separation rates than other models, requiring smaller times to reach a similar level of morphology evolution, as observed in Figs. 5–13.

Similar patterns of evolution of the phase separation process are predicted by the three models. Solvent and non-solvent inter-diffuse rapidly, while the polymer remains almost completely in the film region. The polymer is not prevented from moving towards the non-solvent bath, but remains in the bottom area due to the free energy barrier and its low mobility. After this step, surface-directed phase separation (SDPS) process occurs [64–66]. The propagation of the interface at the top of the films may be noted, clearly, which is characteristic of the SDPS mechanism. The influence of this mechanism is restrict to a finite distance close to the non-solvent bath; in the region below the interface is observed delayed bulk spinodal decomposition compared to SDPS. In early stage of bulk spinodal decomposition process is noticed that the polymer phases separate in a co-continuous morphology.

In the first instants, the structures are noticeably non-uniform due to surface-directed phase separation process. But in the course of the phase separation process, morphologies tend to become uniform: the upper layers formed by SDPS separate into smaller regions. The modified DO and TW models present a higher speed in this process. Some upper layers generated by the CH model do not separate in smaller regions.

Polymer ternary systems undergoing spinodal decomposition exhibit two morphologies, particulate and co-continuous. The particulate morphology (dispersed phase) usually consists of spheres or reasonable approximations of spheres; sometimes can be oriented (ellipsoidal domains). In some simulations, a particulate morphology can be observed in the late stages of bulk spinodal decomposition. This is related to initial polymer concentration: an increase of polymer volume fraction in the film results in change at morphology from isolated droplets (particulate) to co-continuous pattern. In contrast, as observed by Zhou and Powell [24], the increase of the solvent volume fraction does not cause difference in the morphological structure, but cause increment in size of polymer-rich microdomains. In all tests, on late stages of spinodal decomposition, the domains grow in size but retain the same shapes, being approximately self-similar.

The models were also able of identifying differences of phase separation rate and morphology evolution between the three considered polymeric systems. Phase separation for the CA system is much slower

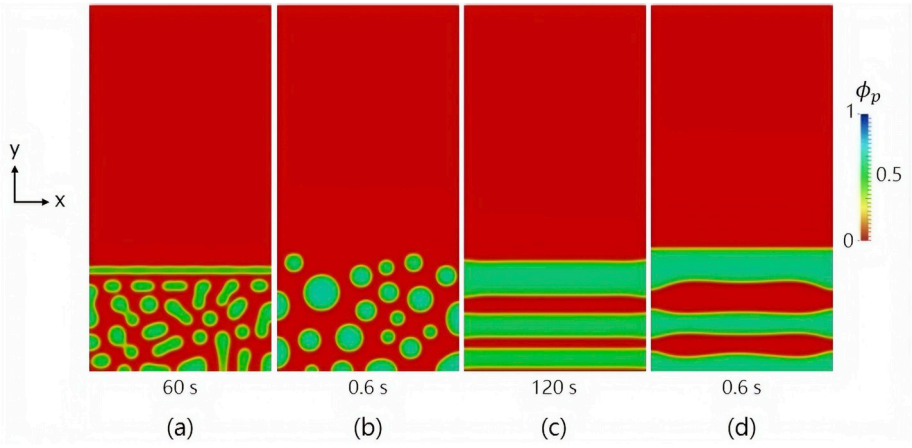

Fig. 4. Morphology of water/acetone/CA with different initial concentrations and mobilities predict by DO model: (a) $\{\varphi_s,\ \varphi_p\} = \{0.2, 0.2\}$, $M_p = 7.22 \times 10^{-22}$ m^5 J^{-1} s^{-1} (b) $\{\varphi_s,\ \varphi_p\} = \{0.2, 0.2\}$, $M_p = 3.61 \times 10^{-19}$ m^5 J^{-1} s^{-1}; (c) $\{\varphi_s,\ \varphi_p\} = \{0.55, 0.4\}$, $M_p = 7.22 \times 10^{-22}$ m^5 J^{-1} s^{-1}; (d) $\{\varphi_s,\ \varphi_p\} = \{0.55, 0.4\}$, $M_p = 3.61 \times 10^{-19}$ m^5 J^{-1} s^{-1}. The bath concentration is essentially pure non-solvent: $\{\varphi_s,\ \varphi_p\} = \{0.01, 0.01\}$.

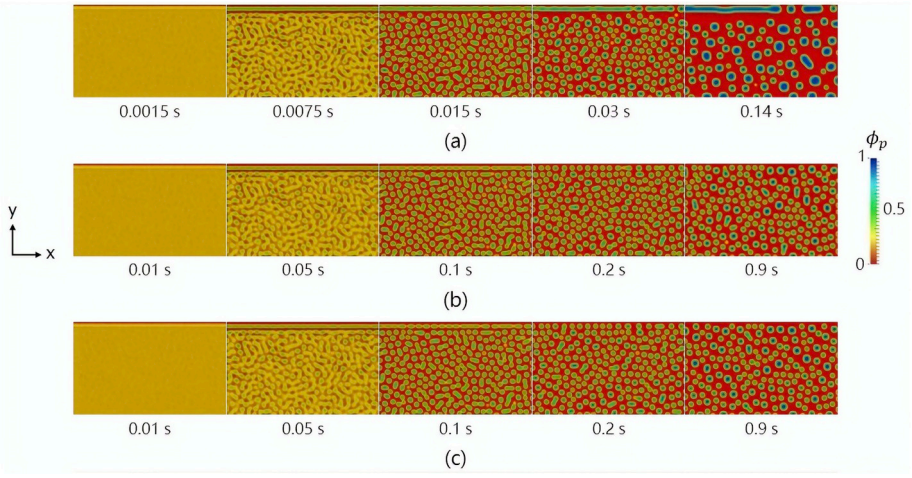

Fig. 5. Morphological evolution of φ_p for the test A1: (a) CH; (b) modified DO; (c) TW. System analyzed: water/DMF/PVDF. The bath concentration is essentially pure non-solvent: $\{\varphi_s,\ \varphi_p\} = \{0.01, 0.01\}$. The polymer solution concentration is: $\{\varphi_s,\ \varphi_p\} = \{0.2, 0.2\}$.

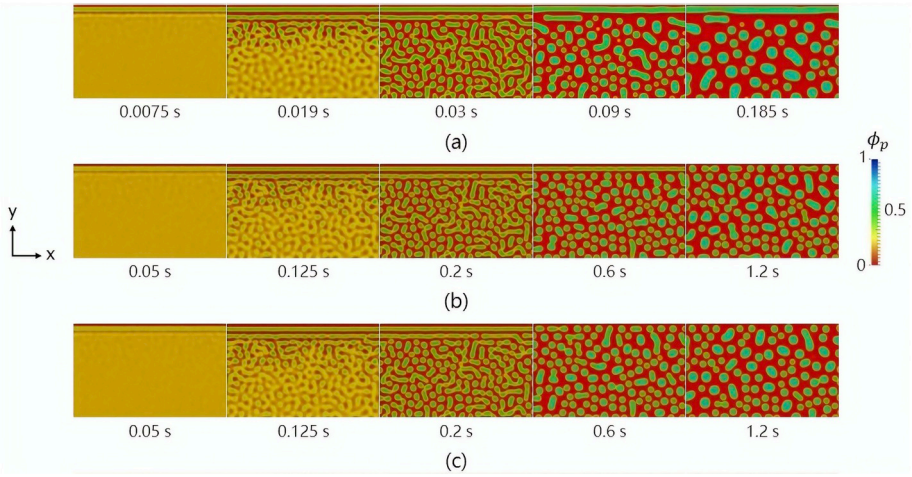

Fig. 6. Morphological evolution of φ_p for the test A2: (a) CH; (b) modified DO; (c) TW. System analyzed: water/DMF/PVDF. The bath concentration is essentially pure non-solvent: $\{\varphi_s,\ \varphi_p\} = \{0.01, 0.01\}$. The polymer solution concentration is: $\{\varphi_s,\ \varphi_p\} = \{0.75, 0.2\}$.

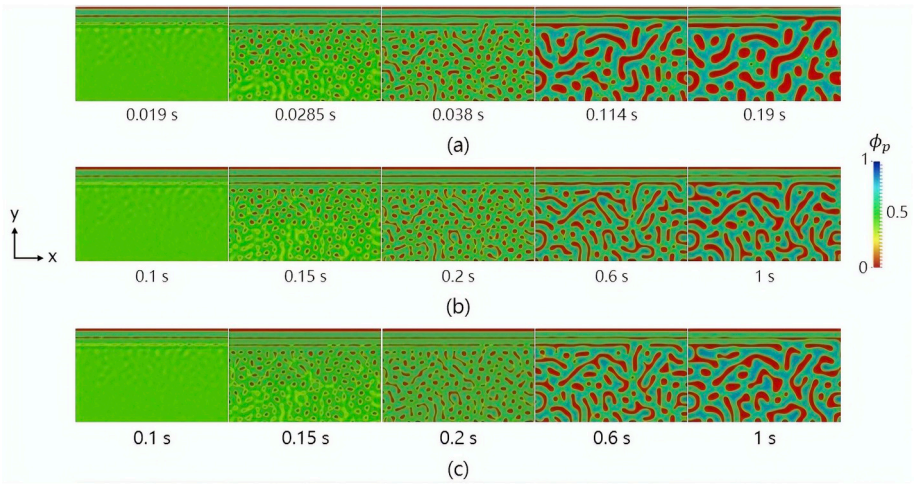

Fig. 7. Morphological evolution of φ_p for the test A3: (a) CH; (b) modified DO; (c) TW. System analyzed: water/DMF/PVDF. The bath concentration is essentially pure non-solvent: $\{\varphi_s,\ \varphi_p\} = \{0.01, 0.01\}$. The polymer solution concentration is: $\{\varphi_s,\ \varphi_p\} = \{0.55, 0.4\}$.

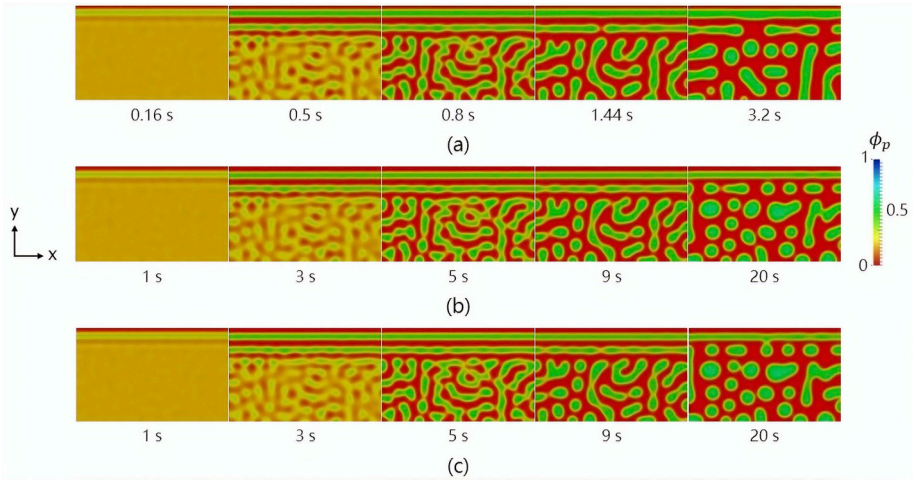

Fig. 8. Morphological evolution of φ_p for the test B1: (a) CH; (b) modified DO; (c) TW. System analyzed: water/acetone/CA. The bath concentration is essentially pure non-solvent: $\{\varphi_s,\ \varphi_p\} = \{0.01, 0.01\}$. The polymer solution concentration is: $\{\varphi_s,\ \varphi_p\} = \{0.7, 0.2\}$.

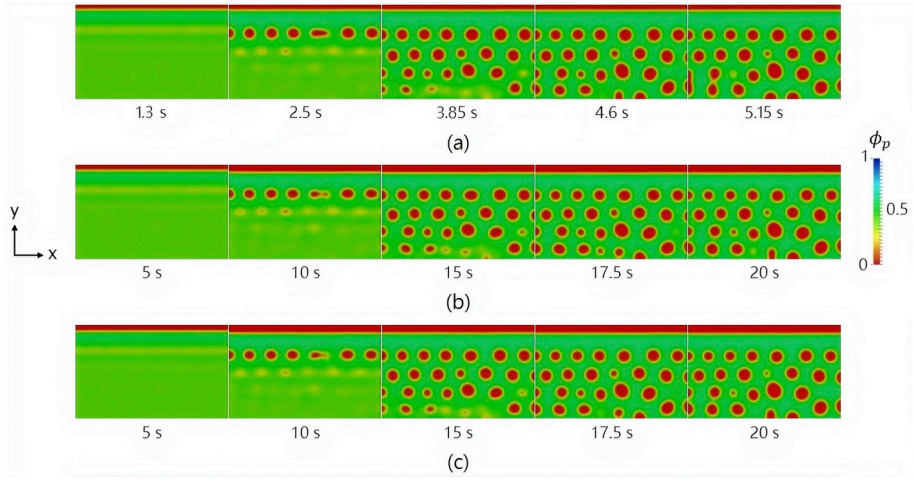

Fig. 9. Morphological evolution of φ_p for the test B2: (a) CH; (b) modified DO; (c) TW. System analyzed: water/acetone/CA. The bath concentration is essentially pure non-solvent: $\{\varphi_s,\ \varphi_p\} = \{0.01, 0.01\}$. The polymer solution concentration is: $\{\varphi_s,\ \varphi_p\} = \{0.55, 0.4\}$..

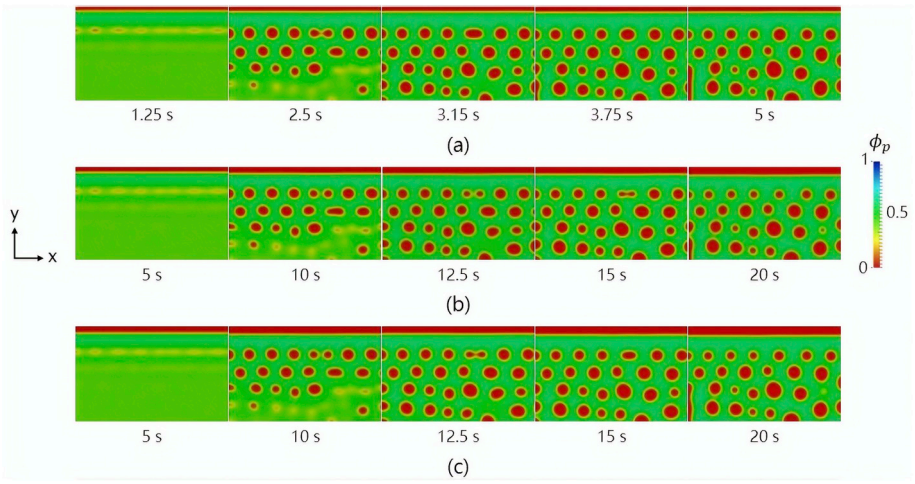

Fig. 10. Morphological evolution of φ_p for the test B3: (a) CH; (b) modified DO; (c) TW. System analyzed: water/acetone/CA. The bath concentration is essentially pure non-solvent: $\{\varphi_s,\ \varphi_p\} = \{0.01, 0.01\}$. The polymer solution concentration is: $\{\varphi_s,\ \varphi_p\} = \{0.4, 0.4\}$.

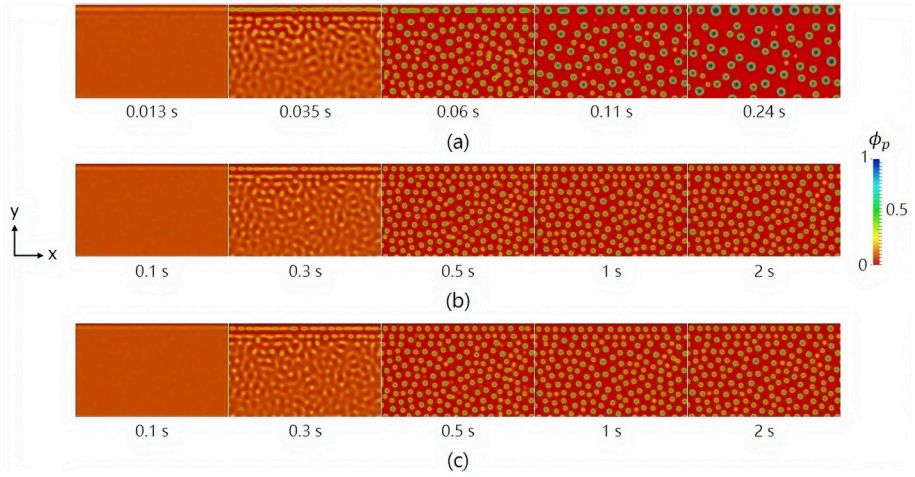

Fig. 11. Morphological evolution of φ_p for the test C1: (a) CH; (b) modified DO; (c) TW. System analyzed: water/DMSO/PES. The bath concentration is essentially pure non-solvent: $\{\varphi_s,\ \varphi_p\} = \{0.01, 0.01\}$. The polymer solution concentration is: $\{\varphi_s,\ \varphi_p\} = \{0.85, 0.1\}$.

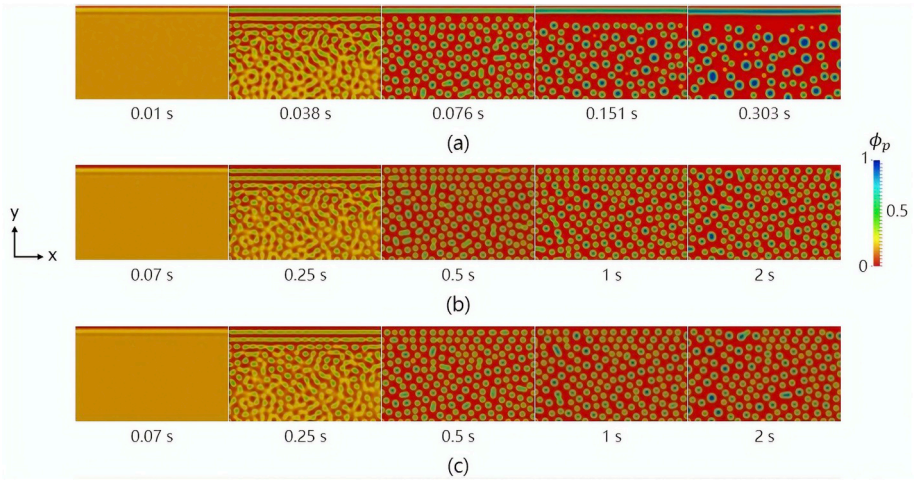

Fig. 12. Morphological evolution of φ_p for the test C2: (a) CH; (b) modified DO; (c) TW. System analyzed: water/DMSO/PES. The bath concentration is essentially pure non-solvent: $\{\varphi_s,\ \varphi_p\} = \{0.01, 0.01\}$. The polymer solution concentration is: $\{\varphi_s,\ \varphi_p\} = \{0.775, 0.175\}$.

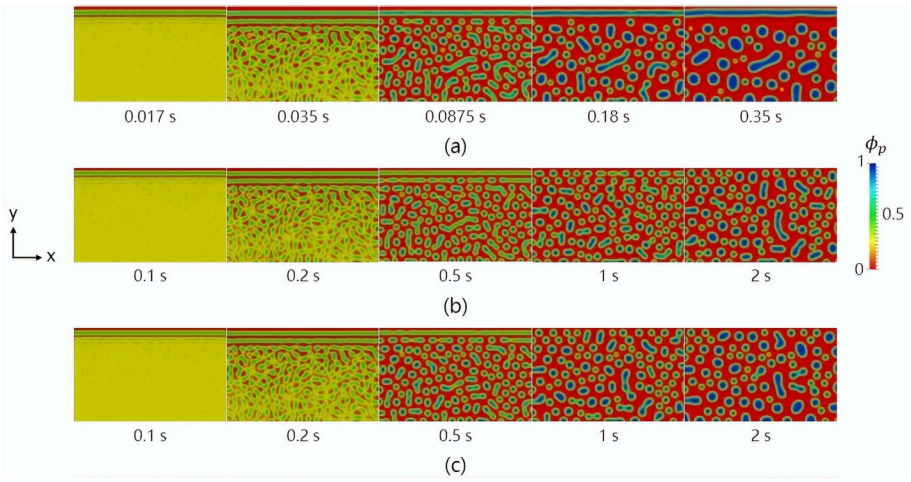

Fig. 13. Morphological evolution of φ_p for the test C3: (a) CH; (b) modified DO; (c) TW. System analyzed: water/DMSO/PES. The bath concentration is essentially pure non-solvent: $\{\varphi_s,\ \varphi_p\} = \{0.01, 0.01\}$. The polymer solution concentration is: $\{\varphi_s,\ \varphi_p\} = \{0.7, 0.25\}$.

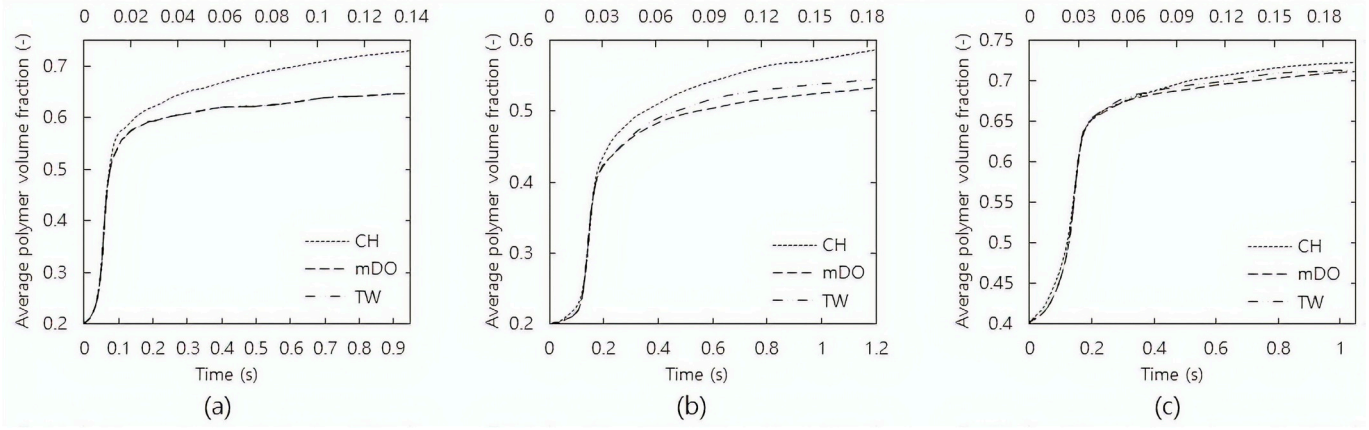

Fig. 14. Average polymer volume fraction in the rich phase: (a) test A1; (b) test A2; (c) test A3. System analyzed: water/DMF/PVDF. The bath concentration is essentially pure non-solvent: $\{\varphi_s,\ \varphi_p\} = \{0.01, 0.01\}$. The polymer solution concentrations are: (a) $\{\varphi_s,\ \varphi_p\} = \{0.2, 0.2\}$; (b) $\{\varphi_s,\ \varphi_p\} = \{0.75, 0.2\}$; (c) $\{\varphi_s,\ \varphi_p\} = \{0.55, 0.4\}$. Upper scale indicates phase separation time by CH model.

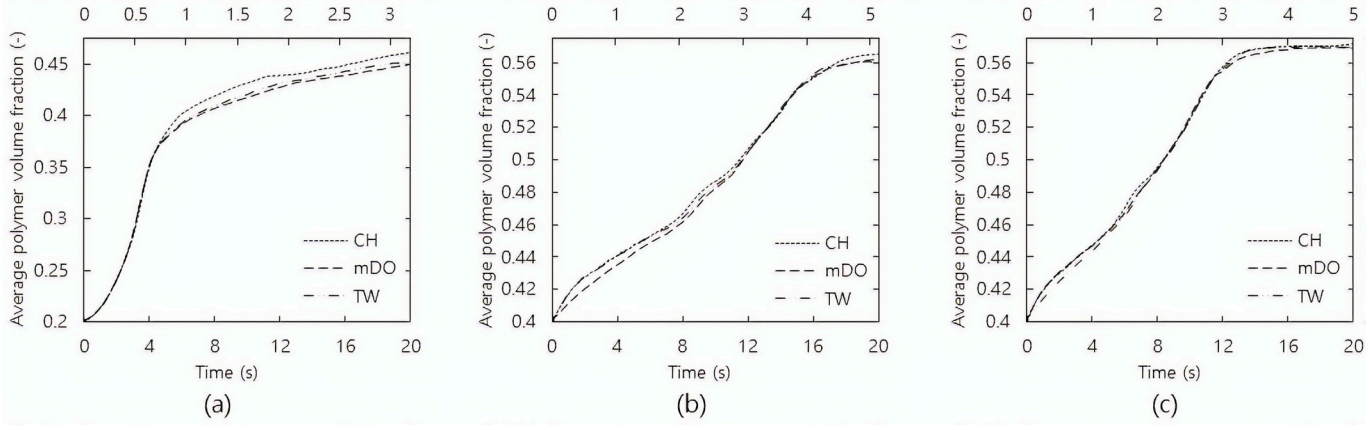

Fig. 15. Average polymer volume fraction in the rich phase: (a) test B1; (b) test B2; (c) test B3. System analyzed: water/acetone/CA. The bath concentration is essentially pure non-solvent: $\{\varphi_s,\ \varphi_p\} = \{0.01, 0.01\}$. The polymer solution concentrations are: (a) $\{\varphi_s,\ \varphi_p\} = \{0.7, 0.2\}$; (b) $\{\varphi_s,\ \varphi_p\} = \{0.55, 0.4\}$; (c) $\{\varphi_s,\ \varphi_p\} = \{0.4, 0.4\}$. Upper scale indicates phase separation time by CH model.

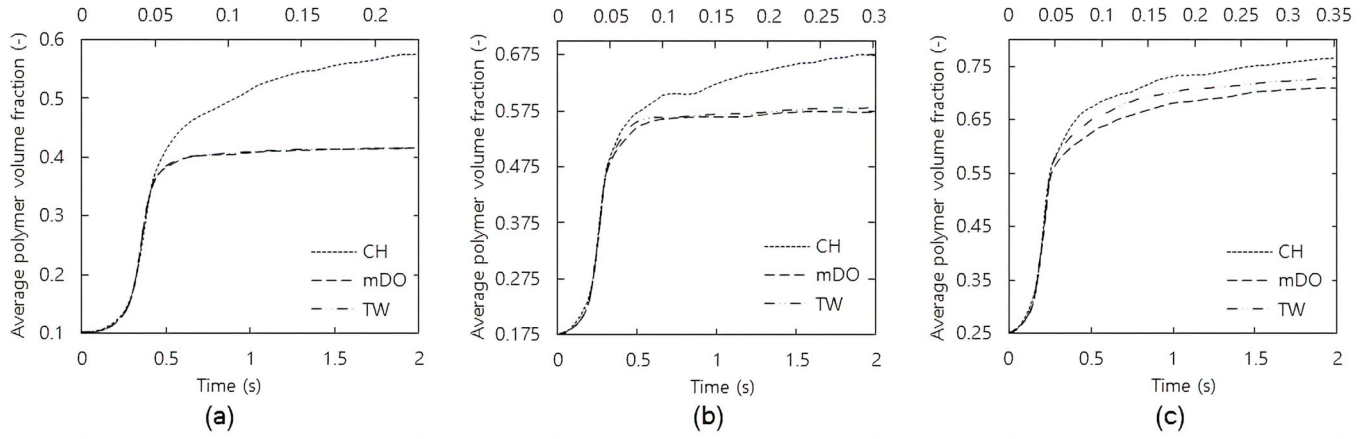

Fig. 16. Average polymer volume fraction in the rich phase: (a) test C1; (b) test C2; (c) test C3. System analyzed: water/DMSO/PES. The bath concentration is essentially pure non-solvent: $\{\varphi_s,\ \varphi_p\} = \{0.01, 0.01\}$. The polymer solution concentrations are: (a) $\{\varphi_s,\ \varphi_p\} = \{0.85, 0.1\}$; (b) $\{\varphi_s,\ \varphi_p\} = \{0.775, 0.175\}$; (c) $\{\varphi_s,\ \varphi_p\} = \{0.7, 0.25\}$. Upper scale indicates phase separation time by CH model.

than it was for the PVDF and PES systems, which can be understood in terms of its smaller χ_{np} value. Despite the tests A3 (water/DMF/PVDF) and B2 (water/acetone/CA) had the same initial concentrations, they presented distinct morphologies: co-continuous pattern and isolated droplets, respectively.

The average polymer volume fraction in the polymer-rich phases (φ_{p_m}) was used as a metric to quantitatively compare the models analyzed. In Figs. 14–16, the polymer volume fraction in the rich phase was plotted as a function of time. From these figures, it can be clearly seen that the phase separation process occurs into three stages: initial, intermediate and final. During the initial stage, φ_{p_m} remains approximately constant, i.e., there is no phase separation. In this step practically only the mass transfer between the solvent and the non-solvent occurs. In the next stage, intermediate, the average polymer volume fraction in the rich phase changes rapidly. In the final stage, φ_{p_m} increases more slowly, tending asymptotically to equilibrium concentration (domain concentrations are near the binodal values). As the phase separation evolution predicted by the CH model is much faster than that predicted by the modified DO and TW models, simulation times plotted in Figs. 14–16 were adjusted so that the three stages of the phase separation process were in the same regions on graphs. The curves of all models studied presented, apparently, the same inclinations at

Table 3
Average characteristic length of microstructures generated by models for the final stage[a].

Model		A1	A2	A3	B1	B2	B3	C1	C2	C3
TW	t (s)	1	1.2	1.05	20	20	20	2	2	2
	l_a (μm)	0.114	0.143	0.162	0.253	0.267	0.253	0.089	0.119	0.166
mDO[b]	t (s)	1	1.2	1.05	20	20	20	2	2	2
	l_a (μm)	0.110	0.136	0.158	0.255	0.268	0.255	0.089	0.118	0.160
	dp[c]	3.51	4.90	2.47	0.79	0.37	0.79	0	0.84	3.61
	t_c[d]	−1.87	−1.82	−0.32	0.13	0.08	0.13	0	−0.50	−1.07
	CI[e,f] of t_t[g]	±1.97	±1.97	±2.08	±2.02	±2.03	±2.02	±1.97	±1.97	±1.98
CH	t (s)	0.143	0.185	0.2	3.25	5.15	5	0.23	0.303	0.35
	l_a (μm)	0.149	0.171	0.224	0.260	0.277	0.269	0.138	0.147	0.191
	dp[c]	30.7	19.6	38.3	2.77	3.75	6.32	55.1	23.5	11.4
	t_c[d]	8.38	3.77	3.69	0.59	0.75	1.19	11.2	4.86	1.79
	CI[e,f] of t_t[g]	±1.99	±2.00	±2.06	±2.04	±2.03	±2.02	±2.00	±2.00	±2.01

[a] Systems analyzed: water/DMF/PVDF in A1, A2 and A3; water/DMF/PVDF in B1, B2 and B3; water/DMF/PVDF in C1, C2 and C3. The bath concentration is essentially pure non-solvent: $\{\varphi_s,\ \varphi_p\} = \{0.01, 0.01\}$. The polymer solution concentrations are: A1 $\{\varphi_s,\ \varphi_p\} = \{0.2, 0.2\}$; A2 $\{\varphi_s,\ \varphi_p\} = \{0.75, 0.2\}$; A3 $\{\varphi_s,\ \varphi_p\} = \{0.55, 0.4\}$; B1 $\{\varphi_s,\ \varphi_p\} = \{0.7, 0.2\}$; B2 $\{\varphi_s,\ \varphi_p\} = \{0.55, 0.4\}$; B3 $\{\varphi_s,\ \varphi_p\} = \{0.4, 0.4\}$; C1 $\{\varphi_s,\ \varphi_p\} = \{0.85, 0.1\}$; C2 $\{\varphi_s,\ \varphi_p\} = \{0.775, 0.175\}$; C3 $\{\varphi_s,\ \varphi_p\} = \{0.7, 0.25\}$.

[b] modified DO.

[c] percentage deviation: $dp = 100\dfrac{|l_{atest} - l_{ar}|}{l_{ar}}$.

[d] t calculated: $t_c = \dfrac{l_{atest} - l_{ar}}{\sqrt{\dfrac{\sigma^2_{test}}{n_{test}} + \dfrac{\sigma^2_r}{n_r}}}$, where σ^2 is the variance and n is the amount of data.

[e] confidence interval - 95% confidence.

[f] degree of freedom: $\upsilon_t = \dfrac{\left(\dfrac{\sigma^2_{test}}{n_{test}} + \dfrac{\sigma^2_r}{n_r}\right)^2}{\dfrac{\left(\dfrac{\sigma^2_{test}}{n_{test}}\right)^2}{n_{test} - 1} + \dfrac{\left(\dfrac{\sigma^2_r}{n_r}\right)^2}{n_r - 1}}$.

[g] t table.

initial and intermediate stages. Only at the final stage, the curve slopes are different. The CH model exhibited a larger slope in its curves, providing a higher polymer volume fraction. In relation to the other two models, the proposed model predicted a higher level of phase separation than the modified DO model.

The proposed model was also compared to other models with relation to the average characteristic length of microstructures at the final stage, which are shown in Table 3. In the cases of test A3, B2 and B3, the characteristic lengths measured correspond to the polymer-poor phase; while in the other tests they correspond to the polymer-rich phase. Although the simulation time scales are different, the average characteristic lengths of the microdomains generated by the CH model were higher than those of modified DO and TW models, with exception of tests B1, B2 and B3 (no significant differences among them). The modified DO and TW models present similar values. Furthermore, differences in microstructure lengths due to different initial composition values are perceived. The elevation of initial polymer volume fraction, maintaining the polymer-rich phase like isolated structure, produced an increase in the characteristic lengths (test C1, C2 and C3).

In summary, the proposed model predicts results significantly different from CH and DO models. The CH model developed by Zhou and Powell [24] ignores the Gibbs-Duhem relation and volume fraction constraint in calculating the diffusion potential and despises the components fluxes dependence with φ_i. These mistakes cause greater phase separation rates and higher characteristic lengths of microdomains. DO model indicated by Tree et al. [30] provides adequate phase separation results only when polymer initial concentrations are inside the spinodal region. If the initial volume fractions are in the stable region, this model may predict the formation of a layered structure, which is not verified in polymer membranes. DO model must be modified to present coherent results, using different mobilities in the components diffusion equations.

5. Conclusions

We presented a new approach to the phase-field model for the phase separation dynamics in polymer membrane formation by the NIPS process, with the aim of better understanding of polymer morphology development. The proposed model consistency was checked by the law of mass conservation and thermodynamically: component volume fractions are conserved in simulations and equilibrium concentrations provide excellent agreement with the associated ternary phase diagram. This new approach of phase-field model was compared to two models previously published in the literature, the Doi-Onuki (DO) and classic Cahn-Hilliard (CH) models. Our approach offers significantly different results in relation to these models. Differently of the DO model, the application of the proposed model was not restricted to values of initial polymer concentration inside the spinodal region, because different mobilities for the polymer and solvent were used. In comparison to the CH model, the main difference observed was the prediction of lower phase separation rates and minor characteristic lengths of microdomains, because it considers the Gibbs-Duhem relation and volume fraction constraint in the calculation of the driving force for diffusion and the influence of the volume fraction on the diffusive flux of the components. Based on these results, the proposed model can be indicated as appropriate for modeling the diffusion effect during polymer membrane formation and can be explored further in future research.

Author contribution statement

Erlí José Padilha Júnior: Conceptualization, Methodology, Software, Validation, Formal analysis, Writing- Original draft preparation; Paula Bettio Staudt: Conceptualization, Methodology, Validation, Writing-Reviewing and Editing; Isabel Cristina Tessaro: Conceptualization, Methodology, Validation, Supervision, Writing- Reviewing and Editing; Nilo Sérgio Medeiros Cardozo: Conceptualization, Methodology, Validation, Supervision, Writing- Reviewing and Editing.

Declaration of competing interest

None.

Acknowledgments

The authors acknowledge computational support from CESUP/UFRGS.

References

[1] M. Amirilargani, M. Sadrzadeh, E.J.R. Sudhölter, L.C.P.M. de Smet, Surface modification methods of organic solvent nanofiltration membranes, Chem. Eng. J. 289 (2016) 562–582, https://doi.org/10.1016/j.cej.2015.12.062.
[2] M. Kamali, D.P. Suhas, M.E. Costa, I. Capela, T.M. Aminabhavi, Sustainability considerations in membrane-based technologies for industrial effluents treatment, Chem. Eng. J. 368 (2019) 474–494, https://doi.org/10.1016/j.cej.2019.02.075.
[3] M. Mulder, Basic Principles of Membrane Technology, second ed., Kulwer Academic Publishers, Dordrecht, 1996.
[4] P. van de Witte, P.J. Dijkstra, J.W.A. van den Berg, J. Feijen, Phase separation processes in polymer solutions in relation to membrane formation, J. Membr. Sci. 117 (1996) 1–31, https://doi.org/10.1016/0376-7388(96)00088-9.
[5] C. Cohen, G.B. Tanny, S. Prager, Diffusion-controlled formation of porous structures in ternary polymer systems, J. Polym. Sci., Polym. Phys. Ed. 17 (1979) 477–489, https://doi.org/10.1002/pol.1979.180170312.
[6] L. Yilmaz, A.J. McHugh, Modelling of asymmetric membrane formation. I. Critique of evaporation models and development of a diffusion equation formalism for the quench period, J. Membr. Sci. 28 (1986) 287–310, https://doi.org/10.1016/S0376-7388(00)82040-2.
[7] L. Yilmaz, A.J. McHugh, Modeling of asymmetric membrane formation. II. The effects of surface boundary conditions, J. Appl. Polym. Sci. 35 (1988) 1967–1979, https://doi.org/10.1002/app.1988.070350722.
[8] A.J. Reuvers, J.W.A. Van den Berg, C.A. Smolders, Formation of membranes by means of immersion precipitation: Part I. A model to describe mass transfer during immersion precipitation, J. Membr. Sci. 34 (1987) 45–65, https://doi.org/10.1016/S0376-7388(00)80020-4.
[9] A.J. Reuvers, C.A. Smolders, Formation of membranes by means of immersion precipitation: Part II. The mechanism of formation of membranes prepared from the system cellulose acetate-acetone-water, J. Membr. Sci. 34 (1987) 67–86, https://doi.org/10.1016/S0376-7388(00)80021-6.
[10] C.S. Tsay, A.J. McHugh, Mass transfer modeling of asymmetric membrane formation by phase inversion, J. Polym. Sci. B Polym. Phys. 28 (1990) 1327–1365, https://doi.org/10.1002/polb.1990.090280810.
[11] P. Radovanovic, S.W. Thiel, S.T. Hwang, Formation of asymmetric polysulfone membranes by immersion precipitation. Part I. Modelling mass transport during gelation, J. Membr. Sci. 65 (1992) 213–229, https://doi.org/10.1016/0376-7388(92)87024-R.
[12] P. Radovanovic, S.W. Thiel, S.T. Hwang, Formation of asymmetric polysulfone membranes by immersion precipitation. Part II. The effects of casting solution and gelation bath compositions on membrane structure and skin formation, J. Membr. Sci. 65 (1992) 231–246, https://doi.org/10.1016/0376-7388(92)87025-S.
[13] L.-P. Cheng, Y.S. Soh, A.-H. Dwan, C.C. Gryte, An improved model for mass transfer during the formation of polymeric membranes by the immersion-precipitation process, J. Polym. Sci. B Polym. Phys. 32 (1994) 1413–1425, https://doi.org/10.1002/polb.1994.090320813.
[14] Y. Termonia, Monte Carlo diffusion model of polymer coagulation, Phys. Rev. Lett. 72 (1994) 3678–3681, https://doi.org/10.1103/PhysRevLett.72.3678.
[15] Y. Termonia, Molecular modeling of phase-inversion membranes: effect of additives in the coagulant, J. Membr. Sci. 104 (1995) 173–180, https://doi.org/10.1016/0376-7388(95)00032-8.
[16] W.F.C. Kools, PhD thesis, Universiteit Twente, 1998.
[17] B.F. Barton, P.D. Graham, A.J. McHugh, Dynamics of spinodal decomposition in polymer solutions near a glass transition, Macromolecules 31 (1998) 1672–1679, https://doi.org/10.1021/ma970964j.
[18] B.F. Barton, A.J. McHugh, Kinetics of thermally induced phase separation in ternary polymer solutions. Part I. Modeling of phase separation dynamics, J. Polym. Sci. B Polym. Phys. 37 (1999) 1449–1460, https://doi.org/10.1002/(SICI)1099-0488(19990701)37:13<1449::AID-POLB11>3.0.CO, 2-T.
[19] B.F. Barton, A.J. McHugh, Modeling the dynamics of membrane structure formation in quenched polymer solutions, J. Membr. Sci. 166 (2000) 119–125, https://doi.org/10.1016/S0376-7388(99)00257-4.
[20] G.R. Fernandes, J.C. Pinto, R. Nobrega, Modeling and simulation of the phase-inversion process during membrane preparation, J. Appl. Polym. Sci. 82 (2001) 3026–3051, https://doi.org/10.1002/app.2159.
[21] Y.D. Kim, J.Y. Kim, H.K. Lee, S.C. Kim, A new modeling of asymmetric membrane formation in rapid mass transfer system, J. Membr. Sci. 190 (2001) 69–77, https://doi.org/10.1016/S0376-7388(01)00420-3.
[22] R. Saxena, G.T. Caneba, Study of spinodal decomposition in a ternary polymer–solvent–nonsolvent system, Polym. Eng. Sci. 42 (2002) 1019–1031, https://doi.org/10.1002/pen.11009.
[23] A. Akthakul, C.E. Scott, A.M. Mayes, A.J. Wagner, Lattice Boltzmann simulation of asymmetric membrane formation by immersion precipitation, J. Membr. Sci. 249 (2005) 213–226, https://doi.org/10.1016/j.memsci.2004.09.045.

[24] B. Zhou, A. Powell, Phase field simulations of early stage structure formation during immersion precipitation of polymeric membranes in 2D and 3D, J. Membr. Sci. 268 (2006) 150–164, https://doi.org/10.1016/j.memsci.2005.05.030.
[25] X.-L. Wang, H.-J. Qian, L.-J. Chen, Z.-Y. Lu, Z.-S. Li, Dissipative particle dynamics simulation on the polymer membrane formation by immersion precipitation, J. Membr. Sci. 311 (2008) 251–258, https://doi.org/10.1016/j.memsci.2007.12.024.
[26] H. Lee, W.B. Krantz, S.-T. Hwang, A model for wet-casting polymeric membranes incorporating nonequilibrium interfacial dynamics, vitrification and convection, J. Membr. Sci. 354 (2010) 74–85, https://doi.org/10.1016/j.memsci.2010.02.066.
[27] X. He, C. Chen, Z. Jiang, Y. Su, Computer simulation of formation of polymeric ultrafiltration membrane via immersion precipitation, J. Membr. Sci. 371 (2011) 108–116, https://doi.org/10.1016/j.memsci.2011.01.016.
[28] S. Liu, Z. Jiang, X. He, Computer simulation of the formation of anti-fouling polymeric ultrafiltration membranes with the addition of amphiphilic block copolymers, J. Membr. Sci. 442 (2013) 97–106, https://doi.org/10.1016/j.memsci.2013.04.025.
[29] Y. Mino, T. Ishigami, Y. Kagawa, H. Matsuyama, Three-dimensional phase-field simulations of membrane porous structure formation by thermally induced phase separation in polymer solutions, J. Membr. Sci. 483 (2015) 104–111, https://doi.org/10.1016/j.memsci.2015.02.005.
[30] D.R. Tree, K.T. Delaney, H.D. Ceniceros, T. Iwana, G.H. Fredrickson, A multi-fluid model for microstructure formation in polymer membranes, Soft Matter 13 (2017) 3013–3030, https://doi.org/10.1039/c6sm02839j.
[31] M. Hopp-Hirschler, U. Nieken, Modeling of pore formation in phase inversion processes: model and numerical results, J. Membr. Sci. 564 (2018) 820–831, https://doi.org/10.1016/j.memsci.2018.07.085.
[32] J.W. Cahn, J.E. Hilliard, Free energy of a nonuniform system. I. Interfacial free energy, J. Chem. Phys. 28 (1958) 258–267, https://doi.org/10.1063/1.1744102.
[33] J.W. Cahn, J.E. Hilliard, Free energy of a nonuniform system - II. Thermodynamical basis, J. Chem. Phys. 30 (1959) 1121–1135, https://doi.org/10.1063/1.1730145.
[34] J.W. Cahn, On spinodal decomposition, Acta Metall. 9 (1961) 795–801, https://doi.org/10.1016/0001-6160(61)90182-1.
[35] M. Doi, A. Onuki, Dynamic coupling between stress and composition in polymer solutions and blends, J. Phys. II France 2 (1992) 1631–1656, https://doi.org/10.1051/jp2:1992225.
[36] E.B. Nauman, D.Q. He, Morphology predictions for ternary polymer blends undergoing spinodal decomposition, Polymer 35 (1994) 2243–2255, https://doi.org/10.1016/0032-3861(94)90757-9.
[37] E.B. Nauman, D.Q. He, Nonlinear diffusion and phase separation, Chem. Eng. Sci. 56 (2001) 1999–2018, https://doi.org/10.1016/S0009-2509(01)00005-7.
[38] D.A. Cogswell, W.C. Carter, Thermodynamic phase-field model for microstructure with multiple components and phases: the possibility of metastable phases, Phys. Rev. E 83 (2011), https://doi.org/10.1103/PhysRevE.83.061602, 061602(1)-061602(13).
[39] S. Emmanuel, A. Cortis, B. Berkowitz, Diffusion in multicomponent systems: a free energy approach, Chem. Phys. 302 (2004) 21–30, https://doi.org/10.1016/j.chemphys.2004.03.013.
[40] B. Zhou, PhD thesis, Massachusetts Institute of Technology, 2006.
[41] R.W. Balluffi, S.M. Allen, W.C. Carter, Kinetics of Materials, first ed., Wiley-Interscience, New York, 2005.
[42] F.W. Altena, C.A. Smolders, Calculation of liquid-liquid phase separation in a ternary system of a polymer in a mixture of a solvent and a nonsolvent, Macromolecules 15 (1982) 1491–1497, https://doi.org/10.1021/ma00234a008.
[43] L. Yilmaz, A.J. McHugh, Analysis of nonsolvent–solvent–polymer phase diagrams and their relevance to membrane formation modeling, J. Appl. Polym. Sci. 31 (1986) 997–1018, https://doi.org/10.1002/app.1986.070310404.
[44] J. Barzin, B. Sadatnia, Theoretical phase diagram calculation and membrane morphology evaluation for water/solvent/polyethersulfone systems, Polymer 48 (2007) 1620–1631, https://doi.org/10.1016/j.polymer.2007.01.049.
[45] U.W. Gedde, Polymer Physics, first ed., Springer Science & Business Media, Dordrecht, 2013.
[46] L.A.A. Cruz, M. Castier, R. Nobrega, Modelagem do equilíbrio de fases em sistemas poliméricos, Polímeros 4 (1994) 35–42.
[47] Y. Shang, L. Fang, M. Wei, C. Barry, J. Mead, D. Kazmer, Verification of numerical simulation of the self-assembly of polymer-polymer-solvent ternary blends on a heterogeneously functionalized substrate, Polymer 52 (2011) 1447–1457, https://doi.org/10.1016/j.polymer.2011.01.038.
[48] P.G. de Gennes, Dynamics of fluctuations and spinodal decomposition in polymer blends, J. Chem. Phys. 72 (1980) 4756–4763, https://doi.org/10.1063/1.439809.
[49] E.J. Kramer, P. Green, C.J. Palmstrom, Interdiffusion and marker movements in concentrated polymer-polymer diffusion couple, Polymer 25 (1984) 473–480, https://doi.org/10.1016/0032-3861(84)90205-2.
[50] J.S. Vrentas, J.L. Duda, Diffusion in polymer—solvent systems. I. Reexamination of the free-volume theory, J. Polym. Sci. Polym. Phys. Ed 15 (1977) 403–416, https://doi.org/10.1002/pol.1977.180150302.
[51] J.S. Vrentas, J.L. Duda, Diffusion in polymer–solvent systems. II. A predictive theory for the dependence of diffusion coefficients on temperature, concentration, and molecular weight, J. Polym. Sci. Polym. Phys. Ed 15 (1977) 417–439, https://doi.org/10.1002/pol.1977.180150303.
[52] J.L. Duda, Y.C. Ni, J.S. Vrentas, An equation relating self-diffusion and mutual diffusion coefficients in polymer-solvent systems, Macromolecules 12 (1979) 459–462, https://doi.org/10.1021/ma60069a023.
[53] J.S. Vrentas, C.M. Vrentas, A new equation relating self-diffusion and mutual diffusion coefficients in polymer-solvent systems, Macromolecules 26 (1993) 6129–6131, https://doi.org/10.1021/ma00074a040.
[54] S. Alsoy, J.L. Duda, Modeling of multicomponent drying of polymer films, AIChE J. 45 (1999) 896–905, https://doi.org/10.1002/aic.690450420.
[55] J.M. Zielinski, B.F. Hanley, Practical friction-based approach to modeling multicomponent diffusion, AIChE J. 45 (1999) 1–12, https://doi.org/10.1002/aic.690450102.
[56] M. Dabral, L.F. Francis, L.E. Scriven, Drying process paths of ternary polymer solution coating, AIChE J. 48 (2002) 25–37, https://doi.org/10.1002/aic.690480105.
[57] P.E. Price Jr., I.H. Romdhane, Multicomponent diffusion theory and its applications to polymer-solvent systems, AIChE J. 49 (2003) 309–322, https://doi.org/10.1002/aic.690490204.
[58] P. Debye, Angular dissymmetry of the critical opalescence in liquid mixtures, J. Chem. Phys. 31 (1959) 680–687, https://doi.org/10.1063/1.1730446.
[59] M.V. Ariyapadi, E.B. Nauman, Gradient energy parameters for polymer–polymer–solvent systems and their application to spinodal decomposition in true ternary systems, J. Polym. Sci. B Polym. Phys. 30 (1990) 2395–2409, https://doi.org/10.1002/polb.1990.090281216.
[60] OpenFOAM 2.3.1. https://www.openfoam.org/, 2019. (Accessed 13 August 2019).
[61] ImageJ. https://imagej.nih.gov/ij/, 2019. (Accessed 13 August 2019).
[62] D. Carolan, H.M. Chong, A. Ivankovi, A.J. Kinloch, A.C. Taylor, Co-continuous polymer systems: a numerical investigation, Comput. Mater. Sci. 98 (2015) 24–33, https://doi.org/10.1016/j.commatsci.2014.10.039.
[63] G.T. Caneba, D. Soong, Polymer membrane formation through the thermal-inversion process. 2. Mathematical modeling of membrane structure formation, Macromolecules 18 (1985) 2545–2555, https://doi.org/10.1021/ma00154a032.
[64] R.C. Ball, R.L.H. Essery, Spinodal decomposition and pattern formation near surfaces, J. Phys. Condens. Matter 2 (1990) 10303–10320, https://doi.org/10.1088/0953-8984/2/51/006.
[65] R.A.L. Jones, L.J. Norton, E.J. Kramer, F.S. Bates, P. Wiltzius, Surface-directed spinodal decomposition, Phys. Rev. Lett. 66 (1991) 1326–1329, https://doi.org/10.1103/PhysRevLett.66.1326.
[66] S. Puri, K. Binder, Surface-directed spinodal decomposition: phenomenology and numerical results, Phys. Rev. A 46 (1992) 4487–4489, https://doi.org/10.1103/PhysRevA.46.R4487.